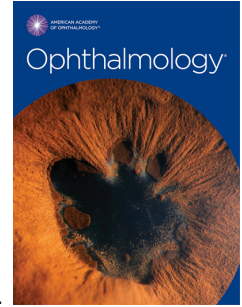


# Journal Pre-proof



Quantitative analysis of optical coherence tomography for neovascular age-related macular degeneration using deep learning

Gabriella Moraes, Dun Jack Fu, Marc Wilson, Hagar Khalid, Siegfried K. Wagner, Edward Korot, Daniel Ferraz, Livia Faes, Christopher J. Kelly, Terry Spitz, Praveen J. Patel, Konstantinos Balaskas, Tiarnan D.L. Keenan, Pearse A. Keane, Reena Chopra

PII: S0161-6420(20)30930-1

DOI: <https://doi.org/10.1016/j.ophtha.2020.09.025>

Reference: OPHTHA 11483

To appear in: *Ophthalmology*

Received Date: 29 June 2020

Revised Date: 25 August 2020

Accepted Date: 21 September 2020

Please cite this article as: Moraes G, Fu DJ, Wilson M, Khalid H, Wagner SK, Korot E, Ferraz D, Faes L, Kelly CJ, Spitz T, Patel PJ, Balaskas K, Keenan TDL, Keane PA, Chopra R, Quantitative analysis of optical coherence tomography for neovascular age-related macular degeneration using deep learning, *Ophthalmology* (2020), doi: <https://doi.org/10.1016/j.ophtha.2020.09.025>.

This is a PDF file of an article that has undergone enhancements after acceptance, such as the addition of a cover page and metadata, and formatting for readability, but it is not yet the definitive version of record. This version will undergo additional copyediting, typesetting and review before it is published in its final form, but we are providing this version to give early visibility of the article. Please note that, during the production process, errors may be discovered which could affect the content, and all legal disclaimers that apply to the journal pertain.

© 2020 Published by Elsevier Inc. on behalf of the American Academy of Ophthalmology

1 **Quantitative analysis of optical coherence tomography for**  
2 **neovascular age-related macular degeneration using deep learning**

---

3  
4 Gabriella Moraes,<sup>1</sup> Dun Jack Fu,<sup>1</sup> Marc Wilson,<sup>2</sup> Hagar Khalid,<sup>1</sup> Siegfried K. Wagner,<sup>1</sup>  
5 Edward Korot,<sup>1</sup> Daniel Ferraz,<sup>1,3</sup> Livia Faes,<sup>1</sup> Christopher J. Kelly,<sup>2</sup> Terry Spitz,<sup>2</sup> Praveen J.  
6 Patel,<sup>1</sup> Konstantinos Balaskas,<sup>1</sup> Tiarnan D. L. Keenan,<sup>4</sup> Pearse A. Keane,<sup>1\*</sup> Reena  
7 Chopra<sup>1,2\*</sup>

8  
9 <sup>1</sup> NIHR Biomedical Research Centre for Ophthalmology, Moorfields Eye Hospital NHS Foundation  
10 Trust and UCL Institute of Ophthalmology, London, United Kingdom

11 <sup>2</sup> Google Health, London, UK

12 <sup>3</sup> Department of Ophthalmology, Federal University São Paulo, São Paulo, Brazil

13 <sup>4</sup> Division of Epidemiology and Clinical Applications, National Eye Institute, National Institutes of  
14 Health, Bethesda, Maryland

15 \* These authors jointly supervised the work

16  
17  
18  
19 **Correspondence and reprint requests:**

20 Pearse A. Keane, MD FRCOphth, NIHR Biomedical Research Centre at Moorfields Eye Hospital NHS  
21 Foundation Trust and UCL Institute of Ophthalmology, London, United Kingdom. Tel: +44 207 523  
22 3411 Fax: +44 207 566 2334 Email: [p.keane@ucl.ac.uk](mailto:p.keane@ucl.ac.uk)

23  
24  
25 This article contains additional online-only material. The following should appear online-only: Supplementary  
26 Material sFigures 1, 2, 3, 4 and 5 and sTables 1, 2, 3, 4, 5 and 6.

27

**28 Abbreviations and Acronyms:**

- 29 Artificial intelligence (AI)
- 30 Age-related macular degeneration (AMD)
- 31 Central subfield thickness (CST)
- 32 Central serous chorioretinopathy (CSCR)
- 33 Confidence interval (CI)
- 34 Early Treatment Diabetic Retinopathy Study (ETDRS)
- 35 External limiting membrane (ELM)
- 36 Fibrovascular pigment epithelial detachment (fvPED)
- 37 Geographic atrophy (GA)
- 38 Hyperreflective foci (HRF)
- 39 Intraretinal fluid (IRF)
- 40 Macular neovascularization (MNV)
- 41 Neurosensory retina (NSR)
- 42 Optical coherence tomography (OCT)
- 43 Pigment epithelium detachment (PED)
- 44 Receiver operating characteristic (ROC)
- 45 Retinal pigment epithelium (RPE)
- 46 Serous pigment epithelial detachment (sPED)
- 47 Standard deviation (SD)
- 48 Subretinal fluid (SRF)
- 49 Subretinal hyperreflective material (SHRM)
- 50 Vascular endothelial growth factor (VEGF)
- 51 Visual acuity (VA)

52

53

**54 Financial Support:**

55 Macular Society Grant, Award number 179050

56

57

**58 Conflict of Interest:**

59 Dr. Keane has acted as a consultant for DeepMind, Roche, Novartis, and Apellis and is an equity  
60 owner in Big Picture Medical. He has received speaker fees from Heidelberg Engineering, Topcon,  
61 Allergan, and Bayer. He is supported by a Moorfields Eye Charity Career Development Award  
62 (R190028A) and a UK Research & Innovation Future Leaders Fellowship (MR/T019050/1). Ms  
63 Chopra receives studentship support from the College of Optometrists, United Kingdom, and is an  
64 employee of Google LLC and owns Alphabet stock. Dr. Kelly, Mr Spitz and Mr Wilson are employees  
65 of Google LLC and own Alphabet stock. Dr. Korot is a consultant for Google Health. Dr. Patel is  
66 supported by the NIHR BRC at Moorfields Eye Hospital and received speaker fees from Bayer and  
67 Novartis UK. Dr. Balaskas has acted as a consultant for Roche and Novartis and received speaker  
68 fees from Novartis, Bayer, Allergan, Alimera, Topcon and Heidelberg Engineering.

69

**70 Running Head:**

71 Quantitative analysis of optical coherence tomography for neovascular AMD using deep learning.

72

73

74

75

76

77

78 **Abstract**

79 **Purpose:** To apply a deep learning algorithm for automated, objective, and comprehensive  
80 quantification of optical coherence tomography (OCT) scans to a large real-world dataset of  
81 eyes with neovascular age-related macular degeneration (AMD), and make the raw  
82 segmentation output data openly available for further research.

83 **Design:** Retrospective analysis of OCT images from the Moorfields Eye Hospital AMD  
84 Database.

85 **Participants:** 2473 first-treated eyes and another 493 second-treated eyes that commenced  
86 therapy for neovascular AMD between June 2012 and June 2017.

87 **Methods:** A deep learning algorithm was used to segment all baseline OCT scans. Volumes  
88 were calculated for segmented features such as neurosensory retina (NSR), drusen, intraretinal  
89 fluid (IRF), subretinal fluid (SRF), subretinal hyperreflective material (SHRM), retinal pigment  
90 epithelium (RPE), hyperreflective foci (HRF), fibrovascular pigment epithelium detachment  
91 (fvPED), and serous PED (sPED). Analyses included comparisons between first and second  
92 eyes, by visual acuity (VA) and by race/ethnicity, and correlations between volumes.

93 **Main outcome measures:** Volumes of segmented features ( $\text{mm}^3$ ), central subfield thickness  
94 (CST) ( $\mu\text{m}$ ).

95 **Results:** In first-treated eyes, the majority had both IRF and SRF (54.7%). First-treated eyes  
96 had greater volumes for all segmented tissues, with the exception of drusen, which was greater  
97 in second-treated eyes. In first-treated eyes, older age was associated with lower volumes for  
98 RPE, SRF, NSR and sPED; in second-treated eyes, older age was associated with lower  
99 volumes of NSR, RPE, sPED, fvPED and SRF. Eyes from black individuals had higher SRF,  
100 RPE and serous PED volumes, compared with other ethnic groups. Greater volumes of the vast  
101 majority of features were associated with worse VA.

102 **Conclusion:** We report the results of large scale automated quantification of a novel range of  
103 baseline features in neovascular AMD. Major differences between first and second-treated  
104 eyes, with increasing age, and between ethnicities are highlighted. In the coming years,

105 enhanced, automated OCT segmentation may assist personalization of real-world care, and the  
106 detection of novel structure-function correlations. These data will be made publicly available for  
107 replication and future investigation by the AMD research community.

## 108 **Introduction**

109 The advent of high-resolution *in vivo* optical coherence tomography (OCT) imaging has driven  
110 research to identify novel anatomical biomarkers in neovascular age-related macular  
111 degeneration (AMD).<sup>1-3</sup> The upsurge in the number of patients requiring OCT scans for optimal  
112 macular disease management, together with increasing OCT scanning density, have become a  
113 challenge.<sup>3</sup> Automated tools that enable detailed analyses, including segmentation and  
114 quantification of features, may improve our understanding of neovascular AMD and could  
115 potentially assist clinicians in making treatment decisions.

116 OCT-derived parameters such as central subfield thickness (CST) have been utilized to  
117 inform retreatment decisions in clinical trials.<sup>4,5</sup> Although basic measurements such as this can  
118 be automatically generated by OCT software algorithms at scale,<sup>6,7</sup> multiple limitations have  
119 questioned their applicability to influence clinical decisions. These include susceptibility to  
120 segmentation errors,<sup>8</sup> limited reproducibility between different OCT devices,<sup>9</sup> and the lack of  
121 detailed information provided by CST measurement alone (which does not distinguish between  
122 neural tissue, retinal fluid, or retinal fluid in different compartments). Much attention has  
123 therefore been given to identifying other OCT parameters for the optimal management of  
124 neovascular AMD.<sup>2</sup> Post hoc analyses of clinical trials<sup>10-13</sup> and real world studies<sup>1</sup> have explored  
125 how certain baseline morphological parameters such as intraretinal fluid (IRF), subretinal fluid  
126 (SRF), subretinal hyperreflective material (SHRM), and pigment epithelium detachment (PED)  
127 may affect the structural and visual outcomes of patients beginning anti-vascular endothelial  
128 growth factor (VEGF) therapy.

129 Clinical trials such as CATT and HARBOR used macular fluid presence as a qualitative  
130 OCT parameter in their retreatment protocols (in the pro re nata arms); this involved the manual

131 detection of IRF or SRF from macular OCT scans.<sup>14,15</sup> However, both qualitative and  
132 quantitative assessments demonstrate high rates of discrepancies between physicians and  
133 reading centre experts, with disagreements on retinal fluid presence on OCT imaging.<sup>15</sup> Recent  
134 advances in deep learning, a subfield of machine learning leveraging artificial neural networks,  
135 have stimulated an upsurge of automatic assessments of the different segmented features  
136 within an OCT volume, especially IRF, SRF, PED and SHRM.<sup>16-18</sup> Prior work using deep  
137 learning for fluid detection and segmentation have demonstrated highly accurate results and laid  
138 important groundwork for potential clinical and research applications.<sup>19-22</sup> Bogunovic *et al.*  
139 conceived the RETOUCH challenge to spur the development of multi-class fluid segmentation  
140 models, recognising that most research to date did not distinguish between the different fluid  
141 types within an OCT scan.<sup>23</sup> This has been considered an important clinical limitation, since  
142 mounting evidence suggests that subtypes of macular fluid have distinct prognostic impacts on  
143 visual outcomes.<sup>23-25</sup>

144 In 2018, an artificial intelligence (AI)-derived system by De Fauw *et al.*<sup>26</sup> demonstrated  
145 applicability in diagnosing and triaging major retinal diseases, including neovascular AMD.<sup>27</sup> In  
146 this report, we applied the system's segmentation network component to the baseline OCT  
147 scans of eyes starting anti-VEGF therapy for neovascular AMD in the Moorfields Eye Hospital  
148 NHS Foundation Trust AMD Database.<sup>28,29</sup> We use these segmentations to quantify a range of  
149 anatomic parameters and disease features, and to explore their potential significance. We also  
150 make these data publicly available for replication and future investigation by the AMD research  
151 community.

## 152 **Methods**

### 153 **Dataset**

154 The Moorfields AMD dataset for this study included all treatment-naive eyes that began anti-  
155 VEGF therapy for neovascular AMD between 1<sup>st</sup> June 2012 and 30<sup>th</sup> June 2017.<sup>27,28</sup> Imaging

156 data included macular OCT scans captured using 3DOCT-2000 devices (Topcon Corp., Tokyo,  
157 Japan) – comprising 128 B-scans covering a volume of 6x6x2.3mm. Patient demographics  
158 recorded in Moorfields' electronic medical record including age, self-reported gender identity  
159 and race/ethnicity, along with associated clinical metadata including visual acuity (VA) in  
160 ETDRS (early treatment diabetic retinopathy study) letters and whether an injection was  
161 administered, was also available for each visit. Whenever an OCT scan was not available on  
162 the exact day of the first injection for the first-treated eye, a scan from up to 14 days prior was  
163 used. Second-treated eyes that sequentially converted to neovascular AMD and started  
164 treatment in the time period of this study were also analysed, with their baseline scan at their  
165 first injection visit used for analysis. Second-treated eyes were not required to have contributed  
166 to the first-treated eye cohort. All eyes were analysed independently. If multiple scans were  
167 present on the same visit, the scan with the lowest volume of mirror and blink artefacts was  
168 selected for analysis. Where neither of these artefacts existed, the scan with the lowest volume  
169 of padding artefact, indicating less manipulation performed by the OCT device software during  
170 post-processing and therefore a cleaner image capture, was selected. Review and analysis of  
171 retrospective anonymised data was approved by the Moorfields Eye Hospital Institutional  
172 Review Board (ROAD17/031) and the research adhered to the tenets of the Declaration of  
173 Helsinki.

## 174 **Segmentation network**

175 All scans were input into the previously described 3D segmentation network.<sup>26</sup> Briefly, the  
176 network automatically predicts segmented features present at each voxel based on a semantic  
177 segmentation architecture. Voxels can be summed and multiplied by the real world voxel size to  
178 provide volumetric measurements of each feature in a 3D scan. For this study, the following  
179 segmented features were analysed: neurosensory retina (NSR), retinal pigment epithelium  
180 (RPE), IRF, SRF, SHRM, hyperreflective foci (HRF), drusen, fibrovascular pigment epithelium  
181 detachment (fvPED), and serous PED (sPED). The NSR volume segmentation excluded the

182 IRF, SRF, and SHRM components. As the segmentation network consists of an ensemble of 5  
183 instances, the average voxel count between the instances was used.<sup>26</sup> Each voxel equated to  
184  $2.60 \times 11.72 \times 47.24 \mu\text{m}$  in the A-scan, B-scan, and C-scan directions, respectively. These  
185 volumes were scaled to  $\text{mm}^3$  for analysis. The CST measurements were defined as average  
186 thickness in the central 1mm diameter circle of the ETDRS grid, measured in  $\mu\text{m}$ .<sup>30</sup> The CST  
187 comprised all segmented features above the RPE to the inner boundary of the NSR, including  
188 SHRM, SRF, HRF, and IRF. For the binary classification of retinal fluid presence, the threshold  
189 at which fluid is definitely present from a clinical perspective was assessed. Two retinal  
190 specialists independently performed the binary classification task for IRF and SRF presence on  
191 a subset of 573 baseline scans, selected for gradability and to ensure coverage of the range of  
192 IRF/SRF segmented by the model. As the segmentation model may contain some noise/error or  
193 sub-clinically relevant segmented volumes, this was important to determine the clinically  
194 relevant minimum voxel count (and the respective volumes) for both segmented features. The  
195 graders agreed on 524/573 (91.4%) of the scans for SRF presence and on 487/573 (85.0%) of  
196 the scans for IRF presence (sFigure 1) (available at [www.aaojournal.org](http://www.aaojournal.org)). Receiver operating  
197 characteristic (ROC) curves were plotted for the diagnostic accuracy of the segmentation model,  
198 using only scans where the retinal specialists agreed. IRF and SRF were defined as present at  
199  $\geq 453$  voxels ( $0.0007\text{mm}^3$ ) and  $\geq 5199$  voxels ( $0.0075\text{mm}^3$ ), respectively, based on the operating  
200 point closest to the upper left corner (sFigure 2). Of 524 scans where the experts agreed on  
201 presence or absence of SRF, the model also agreed in 90.3% of scans. Of 487 scans where the  
202 experts agreed on presence or absence of IRF, the model also agreed in 72.7% of scans  
203 (sFigure 3).

## 204 **Statistical analysis**

205 The mean, standard deviation (SD), median, and interquartile range were calculated for each  
206 segmented feature, separately for first-treated and second-treated eyes. Boxplots were used to  
207 visualise the distribution of feature volumes between subgroups of eyes, according to age,

208 race/ethnicity, VA, and first-treated vs second-treated eyes. These were displayed on a  
209 logarithmic scale to visualise a range in volume that spans several orders of magnitude between  
210 the segmented features. For the primary analyses, the relationships between first and second-  
211 treated eyes, visual acuity and feature volume, and age and feature volume, were assessed.  
212 The distributions of the segmented features were non-normal, as assessed using the Shapiro-  
213 Wilk test. Non-parametric tests were therefore used for statistical analysis. The Mann-Whitney U  
214 test was used to compare observed volumes between first-treated and second-treated eye.  
215 Univariable regression and Spearman's rank correlation were used to examine the associations  
216 between segmented features, and age and VA, respectively. Statistical significance was set at  
217  $P \leq 0.05$ , with Bonferroni correction applied to the statistical tests in the regression and  
218 correlation analyses. The following analyses were considered exploratory. Stepwise  
219 multivariable linear regression was used to determine whether VA could be predicted using  
220 segmented features and demographic data: categorical variables were dummy coded, and  
221 backward elimination of features was used to determine significant variables where  $P \leq 0.05$ .  
222 Kruskal-Wallis and post-hoc Dunn's tests were used for comparisons between ethnicities  
223 grouped into White, Asian, Black, and "Other or Unknown". Spearman's rank correlation  
224 coefficient was used to assess the relationships between paired feature volumes. All analysis  
225 was performed using Python 3.6. De-identified data for this study will be publicly available from  
226 the Dryad Digital Repository. The Moorfields Eye Hospital NHS Foundation Trust also intends to  
227 make the raw data shared with DeepMind openly available to researchers as part of the Ryan  
228 Initiative for Macular Research.<sup>27</sup>  
229

## 230 **Results**

231 A total of 2966 baseline OCT scans from 2966 eyes of 2580 patients were evaluated. Of  
232 these images, 2473 (83.4%) were first-treated eyes and 493 (19.1%) second-treated eyes.  
233 387 individuals contributed both a first and second-treated eye to the analyses. The  
234 demographic characteristics of the patients are presented in Table 1. Example  
235 segmentations are shown in Figure 1. The volumes for each segmented feature are  
236 summarized in Table 2 and Figure 2. These baseline results are similar to those reported by  
237 other studies (sTable 2). The CST values are presented in sTable 3, alongside data collated  
238 from major clinical trials.

### 239 **First-treated versus second-treated eyes**

240 Significant differences in baseline volumes between first-treated and second-treated eyes  
241 were observed for every segmented feature analysed except HRF (Table 2). With the  
242 exception of drusen, first-treated eyes had greater volumes of all features (Figure 2). The  
243 mean CST for first-treated and second-treated eyes was 347.1  $\mu\text{m}$  (SD: 114.3) and 306.1  
244  $\mu\text{m}$  (SD: 85.1), respectively, and was significantly different ( $P < 0.001$ ). Volumes in individuals  
245 with both first and second-treated eyes ( $n=387$ ) are presented in sTable 1.

### 246 **Correlations between segmented features**

247 The coefficients of Spearman's correlation analyses between paired segmented features are  
248 presented as matrices in Figure 3. FvPED and SHRM volumes were moderately and  
249 positively correlated with each other, and with SRF volume, in both first and second-treated  
250 eyes, but poorly correlated with IRF volume in first-treated eyes. RPE volume showed a  
251 moderate positive correlation with NSR and sPED volumes in both sets of eyes.  
252 Hyperreflective foci showed the strongest volumetric correlation with IRF, and vice-versa.

## 254 **Volumes and Visual Acuity**

255 The distributions of segmented features volumes in first-treated eyes, stratified by VA  
256 subgroups, are shown in Figure 4. The mean volumes of first-treated eyes, stratified by VA,  
257 age, and race/ethnicity subgroups, are summarised in sTable 4 and discussed in detail in  
258 the following sections.

259 In first eyes (Table 3), all segmented features had weak negative volumetric  
260 correlations with VA (each  $P < 0.001$ ), with the exception of sPED, RPE and drusen, which  
261 presented weak positive correlations. univariable linear regression analysis showed CST  
262 had the greatest association with VA ( $R^2 = 0.107$ ,  $P < 0.001$ ) of all features considered  
263 (sFigure 4). The strongest volumetric correlation was observed between SHRM and VA for  
264 both first and second-treated eyes ( $r_s = -0.380$ ,  $P < 0.001$  and  $r_s = -0.293$ ,  $P < 0.001$ ,  
265 respectively). Similarly, univariable linear regression showed SHRM had the greatest  
266 association with VA in second-treated eyes ( $R^2 = 0.122$ ,  $P < 0.001$ ) (sFigure 5). Apart from  
267 NSR, sPED, RPE and drusen, which had positive correlations with VA, all other volumes  
268 had weakly negative correlations with VA in second-treated eyes (Table 4). Drusen and  
269 NSR did not remain significant post-Bonferroni correction. SRF and HRF were not found to  
270 be significantly correlated with VA in second-treated eyes.

271 Multivariable linear regression analysis, with VA as the dependent variable, yielded a  
272 model with adjusted  $R^2 = 0.209$  for first eyes. All feature volumes, CST, age, gender, and  
273 race/ethnicity were used in the initial model. Stepwise regression eliminated NSR and  
274 sPED, and all 14 remaining variables were significant ( $P < 0.05$ ) (sTable 5).

275

276

277

278

## 279 Volumes and Age

280 The distributions of segmented feature volumes in first-treated eyes, stratified by age  
281 groups, are shown in Figure 5. Mean volumes of first eyes are summarised in sTable 4.

282 In first-treated eyes (Table 3), weak negative volumetric correlations between age  
283 and RPE ( $r_s=-0.257$ ,  $P<0.001$ ), sPED ( $r_s=-0.218$ ,  $P<0.001$ ), NSR ( $r_s=-0.114$ ,  $P<0.001$ ), and  
284 SRF ( $r_s=-0.140$ ,  $P<0.001$ ), were observed. IRF and drusen were significantly positively  
285 correlated with age ( $r_s=0.171$  and  $r_s=0.117$ , respectively). univariable linear regression  
286 analysis showed RPE had the greatest association with age ( $R^2=0.061$ ,  $P<0.001$ ) of all  
287 features considered. In second-treated eyes (Table 4), parameters that had weak negative  
288 correlations with age were NSR ( $r_s=-0.171$ ,  $P<0.001$ ), RPE ( $r_s=-0.245$ ,  $P<0.001$ ), sPED ( $r_s=-$   
289  $0.209$ ,  $P<0.001$ ), fvPED ( $r_s=-0.111$ ,  $P=0.014$ ) and SRF ( $r_s=-0.174$ ,  $P<0.001$ ). Similar to first  
290 eyes, IRF in second-treated eyes also had a significantly positive correlation with age  
291 ( $r_s=0.190$ ,  $P<0.001$ ). univariable linear regression analysis showed RPE and NSR had the  
292 greatest association with age ( $R^2=0.031$ ,  $P<0.001$  for both segmented features) of all  
293 features considered.

## 294 Volumes and Race/Ethnicity

295 The distributions of segmented feature volumes in the first-treated eyes, stratified by  
296 race/ethnicity, are shown in Figure 6. Mean volumes of first-treated eyes are summarised in  
297 sTable 4. Significant differences in volumes for RPE, SRF, fvPED and sPED were found  
298 between the different ethnic groups. Eyes from black patients had significantly higher  
299 volumes of SRF ( $P<0.05$ ) and RPE ( $P<0.05$ ) than all other groups, and greater sPED  
300 volumes when compared to white and other/unknown ethnicities ( $P<0.05$ ). For fvPED, only  
301 volumes in white patients versus other/unknown patients was significant in post-hoc tests  
302 ( $P<0.05$ ).

303

304

306 The results of the proportion of eyes with IRF and/or SRF present (considered qualitatively,  
307 as present or absent) at baseline are displayed in Table 5. These results were compared to  
308 those from major clinical trials (sTable 6). IRF was present in 66.8% and 60.2% of first and  
309 second-treated eyes, respectively, while SRF was present in 82.7% and 72.6%,  
310 respectively. In first-treated eyes, the majority of eyes had both IRF and SRF (54.7%). For  
311 both sets of eyes, a greater number of eyes had SRF alone (28.0% in first-treated eyes and  
312 33.7% in second-treated eyes) versus IRF alone (12.2% in first-treated eyes and 21.3% in  
313 second-treated eyes).

314

## 315 Discussion

316 The accumulation of vast quantities of imaging data has become both a major challenge and  
317 an exciting opportunity for ophthalmology in the 21st Century. At Moorfields Eye Hospital  
318 alone, there has been a substantial 14-fold increase in the number of OCT scans captured  
319 per year since 2008, from 23,582 scans to 339,639 in 2016.<sup>31</sup> AI, through the use of  
320 machine learning methods, has the potential to revolutionize retinal diagnostics with  
321 techniques that may help optimise disease management and offer the possibility of more  
322 personalised medicine.<sup>24,32,33</sup> In this study, we applied a deep learning-based segmentation  
323 algorithm to OCT scans from the Moorfields AMD Database to automatically identify and  
324 quantify multiple OCT features.

325 IRF, SRF, PEDs and SHRM are important indicators of disease activity in macular  
326 neovascularization (MNV). Using our clinical threshold of fluid presence, the majority of eyes  
327 had both IRF and SRF present at the time of diagnosis in first-treated eyes. The fluid  
328 volumes demonstrated a wide distribution, particularly for IRF, and were likely influenced by  
329 different lesion types,<sup>2,34</sup> the variability of lesion size and activity, differences in speed of

330 patient presentation, and other physiological factors such as VEGF levels, RPE pump  
331 function and integrity of the blood-retinal barriers. Few eyes had IRF alone – likely arising  
332 from type 3 MNV or from VEGF-induced leakage from intraretinal vessels (Figure 1B).<sup>34</sup> IRF  
333 volume had a weak but significant positive correlation with age. Older patients may have a  
334 higher threshold for noticing and acting upon visual symptoms and may either struggle or do  
335 not have the adequate support to access eye care, leading to delayed hospital visits and  
336 later presentation of the disease.<sup>35,36</sup> In addition, these patients may be more likely to have  
337 more IRF than younger patients due to lower external limiting membrane (ELM) integrity  
338 and/or the presence of type 3 MNV. The negative prognostic impact that both increased IRF  
339 and older age independently have on visual outcomes has been well documented.<sup>10,11,28,37</sup>

340         Approximately one-fourth of first-treated eyes had SRF alone, likely representing a  
341 mixture of type 1 MNV (where SRF is thought to be the first exudative sign), and type 2  
342 MNV (particularly when the ELM is intact).<sup>2,34,38</sup> In contrast to IRF, SRF volume had a  
343 significant negative correlation with age. The younger population in our study tended to  
344 demonstrate greater volumes of SRF and sPED. In fact, Black individuals had a significantly  
345 higher volume of SRF and RPE than all other ethnic groups, and more sPED than all other  
346 groups except Asian individuals. Younger patients may be more likely to present sooner, to  
347 have an intact ELM, and to have type 1 or 2 MNV rather than type 3. Some of these cases  
348 may even represent polypoidal choroidal vasculopathy (PCV), which characteristically  
349 presents with SRF and sPED and is more common in younger, and Black and Asian  
350 populations (Figure 1C).<sup>39</sup> This is closely linked to our findings on correlation between  
351 segmented features, where sPED volume showed moderate correlations with both SRF and  
352 RPE volumes.

353         Visual acuity was more strongly associated with IRF than SRF, consistent with  
354 previous studies.<sup>1,3,10,40</sup> Greater IRF volume at baseline has been shown to be more  
355 detrimental to VA than SRF.<sup>1,11,17,41–43</sup> The importance of differentiating among fluid types  
356 has been considered in clinical trials. In the FLUID study, tolerating some SRF, but not IRF,

357 located in VA cases that were non-injected and involved fewer injections. In the current  
358 study, IRF was associated with double the risk of GA development.<sup>44</sup> Consistent with other  
359 reports,<sup>45</sup> there was a moderate negative correlation between VA and SHRM for both first  
360 and second-treated eyes at baseline, supporting the idea that SHRM forms a mechanical  
361 barrier between the RPE and photoreceptors which disrupts the visual cycle.<sup>13</sup>

362 Our comparison between first and second-treated eyes at their first injection visit  
363 revealed that second-treated eyes had significantly smaller volumes of IRF, SRF, SHRM,  
364 fvPED, and sPED, compared to first eyes, suggesting detection at an earlier stage of the  
365 disease. A later presentation in first-treated eyes may be associated with a more advanced  
366 stage of lesion maturity and higher degrees of fibrosis and/or atrophy. This is likely related to  
367 the close surveillance of second-treated eyes whilst first eyes are undergoing treatment;  
368 neovascular conversion in second-treated eyes might be detected at an earlier stage, even  
369 before the onset of visual symptoms.<sup>29,46</sup> Furthermore, systemic absorption of anti-VEGF  
370 drugs has been suggested to decrease VEGF activity in second-treated eyes, possibly  
371 resulting in decreased exudation.<sup>47,48</sup> Drusen was the only segmented feature that  
372 presented greater volumes in second-treated eyes when compared to first-treated eyes  
373 ( $P < 0.05$ ). This could be explained not only by earlier disease detection in second-treated  
374 eyes, but also due to the natural progression of dry AMD prior to conversion, which in both  
375 cases result in a greater drusen volume.

376 In both first and second-treated eyes, fvPED volume correlated moderately with SRF  
377 volume and correlated poorly (first-treated eyes) or did not correlate (second-treated eyes)  
378 with IRF volume. This may relate to the pathophysiology of each fluid type, where SRF  
379 presumably arises directly from a vascularized PED but IRF may come from a vascularized  
380 PED but may also arise from leakage from intraretinal vasculature or a type 3 MNV.<sup>34,38</sup>  
381 Additionally, SHRM volume correlated moderately with SRF volume, which presumably  
382 relates to the broader definition of SHRM as the exudation of various materials such as

383 ceramic, fibrin, and inflammatory cells into the subretinal space, and this being closely  
384 associated with some of these materials.

385 Hyperreflective foci showed the strongest volumetric correlation with IRF, and vice  
386 versa. The origins of HRF in neovascular AMD are unclear, but one hypothesis is that they  
387 represent intraretinal hard exudates secondary to disruption of the blood–retinal barrier,<sup>50</sup>  
388 which could explain their association with IRF. HRF has been shown to be a negative  
389 prognostic indicator and its presence in various retinal layers at baseline have been  
390 associated with poor VA.<sup>51,52</sup> Results from this study show that, although weak, HRF had a  
391 negative correlation with VA at baseline for both first-treated eyes and second-treated eyes.

392 NSR volume had a moderate positive correlation with RPE volume in both first and  
393 second-treated eyes. In cases where macular atrophy accompanies neovascular AMD,  
394 lower volumes of both RPE and NSR might be observed.<sup>34</sup> While in first-treated eyes, NSR  
395 volume was negatively correlated with VA, it was positively correlated in second-treated  
396 eyes. This likely reflects the effect that several different layers may have on NSR thickening  
397 or thinning. On one hand, thickening from non-cystic IRF leads to higher NSR volumes,  
398 while outer retinal atrophy leads to lower NSR volumes, both associated with worse VA.<sup>53,54</sup>  
399 RPE volume was also moderately correlated with SRF volume in both sets of eyes. It has  
400 been proposed that the presence of SRF due to an adjacent perfused neovascular net and  
401 functional choriocapillary layer promotes a favourable environment for a viable RPE.<sup>2</sup> RPE  
402 volumes were significantly positively correlated with VA in both first and second-treated  
403 eyes, reflecting poorer vision in eyes those with RPE loss, and hence atrophy.

404 PED has increasingly been considered a relevant parameter for progressive  
405 neovascular activity. There is no consistent defining criteria for PED among studies, and  
406 most do not classify the PED by subtype.<sup>55</sup> The AI system used in this study automatically  
407 subcategorized PED into fvPED and sPED. The disadvantage of including them within the  
408 same category has been discussed, due to their different effects on visual prognosis, with  
409 sPED at baseline being more associated with PED resolution after anti-VEGF therapy.<sup>56</sup> Our

410 study showed a significant positive association between PED and VA and a significant  
411 negative association between fvPED and VA in first- and second-treated eyes,. As  
412 discussed above, the association of fvPED and poorer VA could be explained by a later  
413 presentation of a more advanced neovascular AMD process. While sPED being more  
414 common in younger age groups, that present at an earlier stage of the disease process,  
415 might correspond to better VA. Drusen being more common in second-treated eyes also  
416 directly correlated with a better VA. While not included in current retreatment protocols, sub-  
417 RPE activity seems to precede degenerative cystic formation, and its recurrence has been  
418 linked to the primary event of neovascular reactivation and long-term vision loss.<sup>57</sup> It has  
419 been suggested that the increase in PED volume during early stages of anti-VEGF therapy  
420 is a useful indicator of fluid recurrence,<sup>58</sup> and the presence of PED may be predictive of  
421 more regular treatment.<sup>55</sup>

422 Central subfield thickness had the highest association with VA in first treated eyes.  
423 At baseline, higher CST usually correlates with poor VA, but this correlation becomes less  
424 evident during follow up.<sup>59,60</sup> Therefore, although used in retreatment decisions of major  
425 clinical trials, its usage has been questioned due to poor reproducibility and lack of  
426 correlation with visual outcomes post treatment.<sup>54</sup> A well known limitation is that the CST  
427 sums several different retinal structures - each structure independently impacting functional  
428 outcomes. One could argue that if IRF, SRF and SHRM all have some degree of negative  
429 correlation with VA, when analysing them together in the form of CST, a stronger  
430 association can be observed compared to analysing each of them individually. However, this  
431 once again highlights the importance of segmenting different features within the total OCT  
432 volume scan.

433 The limitations for this study include its retrospective nature, the variability in the time  
434 that patients present, and the lack of reading centre grading for the individual segmented  
435 features. Additionally, we haven't included the location of the segmented features within the  
436 retinal volume, which could provide further insights into the pathophysiology of the disease

437 and visual prognosis. In future reports, we intend to analyse this further and therefore  
438 provide retinal layer information including axial location, and distance to the foveal centre.  
439 Furthermore, stratifying our cohort to analyse ethnic differences in neovascular AMD  
440 generated unequal group sizes due to the greater prevalence of AMD in White  
441 populations.<sup>62,63</sup> To our knowledge, this is the first study to show the volumetric distribution  
442 of these different segmented features among ethnic groups. Although these results reflect  
443 outcomes from a diverse set of patients from Moorfields Eye Hospital, it does not fully  
444 represent a global population. Considering the epidemiology of AMD as a multifactorial  
445 disease where genetics, race, diet and lifestyle play a role in disease development,  
446 additional studies using diverse datasets would be ideal to compare analyses.

447 The segmentation outputs from this study have been made openly available for the  
448 ophthalmic and AMD research community to download together with this manuscript. This  
449 endorses the worldwide effort to inspire community progress in the healthcare sector. We  
450 compared our results to prior work that calculated tissue and fluid volumes and thicknesses  
451 (sTable 2). Discrepancies observed could arise from differences in methodologies, study  
452 design and data interpretation, for example, the use of different OCT devices and scan  
453 protocols, as well as the difference in cohort demographics. Therefore, making this  
454 comprehensive dataset openly available will be particularly interesting for ophthalmologists  
455 to compare our findings on the baseline OCT characteristics of a large real-world cohort with  
456 those from clinical trials. This could help the clinical community determine whether these  
457 trials have enrolled patients that are representative of real world practice. Additionally, it will  
458 also allow others to replicate our findings as well as conducting their own novel analyses.  
459 Potential clinical uses of the segmentation system may include diagnosis and stratification of  
460 neovascular AMD. In uncertain cases and/or recent conversion to neovascular AMD, the  
461 system could detect and quantify subtle or high risk features of exudation. In addition,  
462 quantification of volumes may aid monitoring efficacy of treatment, provide insight to aid  
463 anti-VEGF drug choice, and help optimize retreatment intervals. Furthermore, the system

464 could allow clinicians to see where the eye in question lies in terms of the usual spectrum of  
465 eyes with neovascular AMD seen in real-world practice.

466 In this study, we presented the results of a large scale analysis using an automated  
467 deep learning 3D segmentation system that classifies and quantifies multiple features within  
468 an OCT volume scan. Our large cohort was extracted from the Moorfields AMD database,  
469 which is perhaps the largest single-centre dataset of neovascular AMD patients.<sup>28</sup>  
470 Automating OCT segmentation will become crucial in further understanding disease  
471 subgroups and quantifying disease progression at a patient level. The characterisation and  
472 quantification of several features may aid personalised medicine and suggest novel  
473 anatomical parameters that can unravel new structure-function correlations in neovascular  
474 AMD.

475

476

477

478

479

480

481

482

483

484

485

486

487

488

- 490 1. Lai T-T, Hsieh Y-T, Yang C-M, Ho T-C, Yang C-H. Biomarkers of optical coherence  
491 tomography in evaluating the treatment outcomes of neovascular age-related macular  
492 degeneration: a real-world study. *Sci Rep.* 2019;9(1):529.
- 493 2. Schmidt-Erfurth U, Waldstein SM. A paradigm shift in imaging biomarkers in  
494 neovascular age-related macular degeneration. *Prog Retin Eye Res.* 2016;50:1-24.
- 495 3. Waldstein SM, Philip A-M, Leitner R, et al. Correlation of 3-Dimensionally Quantified  
496 Intraretinal and Subretinal Fluid With Visual Acuity in Neovascular Age-Related Macular  
497 Degeneration. *JAMA Ophthalmol.* 2016;134(2):182-190.
- 498 4. Fung AE, Lalwani GA, Rosenfeld PJ, et al. An optical coherence tomography-guided,  
499 variable dosing regimen with intravitreal ranibizumab (Lucentis) for neovascular age-  
500 related macular degeneration. *Am J Ophthalmol.* 2007;143(4):566-583.
- 501 5. Lalwani GA, Rosenfeld PJ, Fung AE, et al. A variable-dosing regimen with intravitreal  
502 ranibizumab for neovascular age-related macular degeneration: year 2 of the PrONTO  
503 Study. *Am J Ophthalmol.* 2009;148(1):43-58.e1.
- 504 6. Holz FG, Amoaku W, Donate J, et al. Safety and efficacy of a flexible dosing regimen of  
505 ranibizumab in neovascular age-related macular degeneration: the SUSTAIN study.  
506 *Ophthalmology.* 2011;118(4):663-671.
- 507 7. Boyer DS, Heier JS, Brown DM, Francom SF, Ianchulev T, Rubio RG. A Phase IIIb  
508 study to evaluate the safety of ranibizumab in subjects with neovascular age-related  
509 macular degeneration. *Ophthalmology.* 2009;116(9):1731-1739.
- 510 8. Sadda SR, Wu Z, Walsh AC, et al. Errors in retinal thickness measurements obtained  
511 by optical coherence tomography. *Ophthalmology.* 2006;113(2):285-293.
- 512 9. Waldstein SM, Gerendas BS, Montuoro A, Simader C, Schmidt-Erfurth U. Quantitative  
513 comparison of macular segmentation performance using identical retinal regions across  
514 multiple spectral-domain optical coherence tomography instruments. *Br J Ophthalmol.*  
515 2015;99(6):794-800.
- 516 10. Simader C, Ritter M, Bolz M, et al. Morphologic parameters relevant for visual outcome  
517 during anti-angiogenic therapy of neovascular age-related macular degeneration.  
518 *Ophthalmology.* 2014;121(6):1237-1245.
- 519 11. Waldstein SM, Simader C, Staurenghi G, et al. Morphology and Visual Acuity in  
520 Aflibercept and Ranibizumab Therapy for Neovascular Age-Related Macular  
521 Degeneration in the VIEW Trials. *Ophthalmology.* 2016;123(7):1521-1529.
- 522 12. Waldstein SM, Wright J, Warburton J, Margaron P, Simader C, Schmidt-Erfurth U.  
523 Predictive Value of Retinal Morphology for Visual Acuity Outcomes of Different  
524 Ranibizumab Treatment Regimens for Neovascular AMD. *Ophthalmology.*  
525 2016;123(1):60-69.
- 526 13. Willoughby AS, Ying G-S, Toth CA, et al. Subretinal Hyperreflective Material in the  
527 Comparison of Age-Related Macular Degeneration Treatments Trials. *Ophthalmology.*  
528 2015;122(9):1846-1853.e5.

- 529  
530  
531  
532
14. Ezzouki BS, He H, Brown DM, et al. Fluid Retention, Macular Edema, and Safety of Intravitreal  
2.0 mg Ranibizumab in Patients with Subfoveal Neovascular Age-related Macular  
Degeneration. *Ophthalmology*. 2013;120(5):1046-1056.  
doi:10.1016/j.ophtha.2012.10.014
- 533  
534  
535  
536
15. Toth CA, Decroos FC, Ying G-S, et al. IDENTIFICATION OF FLUID ON OPTICAL  
COHERENCE TOMOGRAPHY BY TREATING OPHTHALMOLOGISTS VERSUS A  
READING CENTER IN THE COMPARISON OF AGE-RELATED MACULAR  
DEGENERATION TREATMENTS TRIALS. *Retina*. 2015;35(7):1303-1314.
- 537  
538  
539  
540
16. Zheng Y, Sahni J, Campa C, Stangos AN, Raj A, Harding SP. Computerized  
assessment of intraretinal and subretinal fluid regions in spectral-domain optical  
coherence tomography images of the retina. *Am J Ophthalmol*. 2013;155(2):277-  
286.e1.
- 541  
542  
543  
544
17. Schmidt-Erfurth U, Vogl W-D, Jampol LM, Bogunović H. Application of automated  
quantification of fluid volumes to anti-VEGF therapy of neovascular age-related macular  
degeneration. *Ophthalmology*. Published online March 16, 2020.  
doi:10.1016/j.ophtha.2020.03.010
- 545  
546  
547
18. Lee H, Kang KE, Chung H, Kim HC. Automated Segmentation of Lesions Including  
Subretinal Hyperreflective Material in Neovascular Age-related Macular Degeneration.  
*Am J Ophthalmol*. 2018;191:64-75.
- 548  
549  
550
19. Li M-X, Yu S-Q, Zhang W, et al. Segmentation of retinal fluid based on deep learning:  
application of three-dimensional fully convolutional neural networks in optical coherence  
tomography images. *Int J Ophthalmol*. 2019;12(6):1012-1020.
- 551  
552  
553
20. Gao K, Niu S, Ji Z, et al. Double-branched and area-constraint fully convolutional  
networks for automated serous retinal detachment segmentation in SD-OCT images.  
*Comput Methods Programs Biomed*. 2019;176:69-80.
- 554  
555  
556
21. Lu D, Heisler M, Lee S, et al. Deep-learning based multiclass retinal fluid segmentation  
and detection in optical coherence tomography images using a fully convolutional  
neural network. *Med Image Anal*. 2019;54:100-110.
- 557  
558  
559
22. Lee CS, Tying AJ, Deruyter NP, Wu Y, Rokem A, Lee AY. Deep-learning based,  
automated segmentation of macular edema in optical coherence tomography. *Biomed  
Opt Express*. 2017;8(7):3440-3448.
- 560  
561  
562
23. Bogunovic H, Venhuizen F, Klmscha S, et al. RETOUCH: The Retinal OCT Fluid  
Detection and Segmentation Benchmark and Challenge. *IEEE Trans Med Imaging*.  
2019;38(8):1858-1874.
- 563  
564  
565
24. Schlegl T, Waldstein SM, Bogunovic H, et al. Fully Automated Detection and  
Quantification of Macular Fluid in OCT Using Deep Learning. *Ophthalmology*.  
2018;125(4):549-558.
- 566  
567  
568  
569
25. Guymer RH, Markey CM, McAllister IL, et al. Tolerating Subretinal Fluid in Neovascular  
Age-Related Macular Degeneration Treated with Ranibizumab Using a Treat-and-  
Extend Regimen: FLUID Study 24-Month Results. *Ophthalmology*. 2019;126(5):723-  
734.
- 570  
571
26. De Fauw J, Ledsam JR, Romera-Paredes B, et al. Clinically applicable deep learning  
for diagnosis and referral in retinal disease. *Nature Medicine*. 2018;24(9):1342-1350.

- 573 27. Yim J, Chopra R, Spitz T, et al. Predicting conversion to wet age-related macular  
574 degeneration using deep learning. *Nat Med*. Published online May 18, 2020.  
575 doi:10.1038/s41591-020-0867-7
- 576 28. Fasler K, Moraes G, Wagner S, et al. One- and two-year visual outcomes from the  
577 Moorfields age-related macular degeneration database: a retrospective cohort study  
578 and an open science resource. *BMJ Open*. 2019;9(6):e027441.
- 579 29. Fasler K, Fu DJ, Moraes G, et al. Moorfields AMD database report 2: fellow eye  
580 involvement with neovascular age-related macular degeneration. *Br J Ophthalmol*.  
581 Published online October 14, 2019. doi:10.1136/bjophthalmol-2019-314446
- 582 30. Huang J, Liu X, Wu Z, Xiao H, Dustin L, Sadda S. Macular thickness measurements in  
583 normal eyes with time-domain and Fourier-domain optical coherence tomography.  
584 *Retina*. 2009;29(7):980-987.
- 585 31. Pontikos N, Wagner SK, Balaskas K, et al. Correspondence: Trends in Retina  
586 Specialist Imaging Utilization From 2012 to 2016 in the United States Medicare Fee-for-  
587 Service Population. *Am J Ophthalmol*. Published online November 15, 2019.  
588 doi:10.1016/j.ajo.2019.09.021
- 589 32. Schmidt-Erfurth U, Sadeghipour A, Gerendas BS, Waldstein SM, Bogunović H. Artificial  
590 intelligence in retina. *Prog Retin Eye Res*. 2018;67:1-29.
- 591 33. Torkamani A, Andersen KG, Steinhubl SR, Topol EJ. High-Definition Medicine. *Cell*.  
592 2017;170(5):828-843.
- 593 34. Spaide RF, Jaffe GJ, Sarraf D, et al. Consensus Nomenclature for Reporting  
594 Neovascular Age-Related Macular Degeneration Data: Consensus on Neovascular  
595 Age-Related Macular Degeneration Nomenclature Study Group. *Ophthalmology*.  
596 Published online 2019.  
597 <https://www.sciencedirect.com/science/article/pii/S0161642019322432>
- 598 35. Owen CG, Jarrar Z, Wormald R, Cook DG, Fletcher AE, Rudnicka AR. The estimated  
599 prevalence and incidence of late stage age related macular degeneration in the UK. *Br*  
600 *J Ophthalmol*. 2012;96(5):752-756.
- 601 36. Sharma HE, Mathewson PA, Lane M, et al. The role of social deprivation in severe  
602 neovascular age-related macular degeneration. *Br J Ophthalmol*. 2014;98(12):1625-  
603 1628.
- 604 37. Holz FG, Tadayoni R, Beatty S, et al. Key drivers of visual acuity gains in neovascular  
605 age-related macular degeneration in real life: findings from the AURA study. *Br J*  
606 *Ophthalmol*. 2016;100(12):1623-1628.
- 607 38. Freund KB, Zweifel SA, Engelbert M. Do we need a new classification for choroidal  
608 neovascularization in age-related macular degeneration? *Retina*. 2010;30(9):1333-  
609 1349.
- 610 39. Cheung CMG, Lai TYY, Ruamviboonsuk P, et al. Polypoidal Choroidal Vasculopathy:  
611 Definition, Pathogenesis, Diagnosis, and Management. *Ophthalmology*.  
612 2018;125(5):708-724.

- 613 40. Lee H, Ji B, Chung H, Kim HC. Three-dimensional analysis of morphologic changes and visual  
614 Outcomes in Neovascular Age-Related Macular Degeneration. *Invest Ophthalmol Vis*  
615 *Sci.* 2017;58(2):1337-1345.
- 616 41. Jaffe GJ, Martin DF, Toth CA, et al. Macular morphology and visual acuity in the  
617 comparison of age-related macular degeneration treatments trials. *Ophthalmology.*  
618 2013;120(9):1860-1870.
- 619 42. Ritter M, Simader C, Bolz M, et al. Intraretinal cysts are the most relevant prognostic  
620 biomarker in neovascular age-related macular degeneration independent of the  
621 therapeutic strategy. *Br J Ophthalmol.* 2014;98(12):1629-1635.
- 622 43. Sharma S, Toth CA, Daniel E, et al. Macular Morphology and Visual Acuity in the  
623 Second Year of the Comparison of Age-Related Macular Degeneration Treatments  
624 Trials. *Ophthalmology.* 2016;123(4):865-875.
- 625 44. Grunwald JE, Daniel E, Huang J, et al. Risk of geographic atrophy in the comparison of  
626 age-related macular degeneration treatments trials. *Ophthalmology.* 2014;121(1):150-  
627 161.
- 628 45. Ristau T, Keane PA, Walsh AC, et al. Relationship between visual acuity and spectral  
629 domain optical coherence tomography retinal parameters in neovascular age-related  
630 macular degeneration. *Ophthalmologica.* 2014;231(1):37-44.
- 631 46. Chevreaud O, Semoun O, Blanco-Garavito R, et al. Visual acuity at presentation in the  
632 second eye versus first eye in patients with exudative age-related macular  
633 degeneration. *Eur J Ophthalmol.* 2016;26(1):44-47.
- 634 47. Peyman M, Peyman A, Lansingh VC, Orandi A, Subrayan V. Intravitreal bevacizumab  
635 versus ranibizumab: Effects on the vessels of the fellow non-treated eye. *J Curr*  
636 *Ophthalmol.* 2019;31(1):55-60.
- 637 48. Avery RL, Castellarin AA, Steinle NC, et al. SYSTEMIC PHARMACOKINETICS AND  
638 PHARMACODYNAMICS OF INTRAVITREAL AFLIBERCEPT, BEVACIZUMAB, AND  
639 RANIBIZUMAB. *Retina.* 2017;37(10):1847-1858. doi:10.1097/iae.0000000000001493
- 640 49. Shah VP, Shah SA, Mrejen S, Freund KB. Subretinal hyperreflective exudation  
641 associated with neovascular age-related macular degeneration. *Retina.*  
642 2014;34(7):1281-1288.
- 643 50. Segal O, Barayev E, Nemet AY, Geffen N, Vainer I, Mimouni M. PROGNOSTIC VALUE  
644 OF HYPERREFLECTIVE FOCI IN NEOVASCULAR AGE-RELATED MACULAR  
645 DEGENERATION TREATED WITH BEVACIZUMAB. *Retina.* 2016;36(11):2175-2182.
- 646 51. Akagi-Kurashige Y, Tsujikawa A, Oishi A, et al. Relationship between retinal  
647 morphological findings and visual function in age-related macular degeneration.  
648 *Graefes Arch Clin Exp Ophthalmol.* 2012;250(8):1129-1136.
- 649 52. Lee H, Ji B, Chung H, Kim HC. CORRELATION BETWEEN OPTICAL COHERENCE  
650 TOMOGRAPHIC HYPERREFLECTIVE FOCI AND VISUAL OUTCOMES AFTER ANTI-  
651 VEGF TREATMENT IN NEOVASCULAR AGE-RELATED MACULAR  
652 DEGENERATION AND POLYPOIDAL CHOROIDAL VASCULOPATHY. *Retina.*  
653 2016;36(3):465-475.
- 654 53. Keane PA, Chang KT, Liakopoulos S, Jivrajka RV, Walsh AC, Sadda SR. Effect of

- 655 ranibizumab retreatment frequency on macular thickness and retinal volume in neovascular  
656 amd. *Retina*. 2009;29(5):592-600.
- 657 54. Keane PA, Liakopoulos S, Chang KT, et al. Relationship between optical coherence  
658 tomography retinal parameters and visual acuity in neovascular age-related macular  
659 degeneration. *Ophthalmology*. 2008;115(12):2206-2214.
- 660 55. Cheong KX, Chong Teo KY, Ming Cheung GC. Influence of pigment epithelial  
661 detachment on visual acuity in neovascular age-related macular degeneration. *Surv*  
662 *Ophthalmol*. Published online May 15, 2020. doi:10.1016/j.survophthal.2020.05.003
- 663 56. Cho HJ, Kim KM, Kim HS, Lee DW, Kim CG, Kim JW. Response of Pigment Epithelial  
664 Detachment to Anti-Vascular Endothelial Growth Factor Treatment in Age-Related  
665 Macular Degeneration. *Am J Ophthalmol*. 2016;166:112-119.
- 666 57. Schmidt-Erfurth U, Waldstein SM, Deak G-G, Kundi M, Simader C. Pigment epithelial  
667 detachment followed by retinal cystoid degeneration leads to vision loss in treatment of  
668 neovascular age-related macular degeneration. *Ophthalmology*. 2015;122(4):822-832.
- 669 58. Penha FM, Gregori G, Garcia Filho CA de A, Yehoshua Z, Feuer WJ, Rosenfeld PJ.  
670 Quantitative changes in retinal pigment epithelial detachments as a predictor for  
671 retreatment with anti-VEGF therapy. *Retina*. 2013;33(3):459-466.
- 672 59. Zhang X, Lai TYY. Baseline Predictors of Visual Acuity Outcome in Patients with Wet  
673 Age-Related Macular Degeneration. *Biomed Res Int*. 2018;2018:9640131.
- 674 60. Ou WC, Brown DM, Payne JF, Wykoff CC. Relationship Between Visual Acuity and  
675 Retinal Thickness During Anti-Vascular Endothelial Growth Factor Therapy for Retinal  
676 Diseases. *Am J Ophthalmol*. 2017;180:8-17.
- 677 61. Wu Z, Cunefare D, Chiu E, et al. Longitudinal Associations Between Microstructural  
678 Changes and Microperimetry in the Early Stages of Age-Related Macular Degeneration.  
679 *Invest Ophthalmol Vis Sci*. 2016;57(8):3714-3722.
- 680 62. Mohamed R, Gadhvi K, Mensah E. What Effect Does Ethnicity Have on the Response  
681 to Ranibizumab in the Treatment of Wet Age-Related Macular Degeneration?  
682 *Ophthalmologica*. 2018;240(3):157-162.
- 683 63. Patel SN, Wu C, Obeid A, et al. Sociodemographic Factors in Neovascular Age-Related  
684 Macular Degeneration. *Ophthalmology*. 2020;127(2):280-282.
- 685 64. Joeres S, Tsong JW, Updike PG, et al. Reproducibility of quantitative optical coherence  
686 tomography subanalysis in neovascular age-related macular degeneration. *Invest*  
687 *Ophthalmol Vis Sci*. 2007;48(9):4300-4307.
- 688 65. Hu X, Waldstein SM, Klmscha S, et al. MORPHOLOGICAL AND FUNCTIONAL  
689 CHARACTERISTICS AT THE ONSET OF EXUDATIVE CONVERSION IN AGE-  
690 RELATED MACULAR DEGENERATION. *Retina*. Published online March 28, 2019.  
691 doi:10.1097/IAE.0000000000002531
- 692 66. Heier JS, Brown DM, Chong V, et al. Intravitreal aflibercept (VEGF trap-eye) in wet age-  
693 related macular degeneration. *Ophthalmology*. 2012;119(12):2537-2548.
- 694 67. CATT Research Group, Martin DF, Maguire MG, et al. Ranibizumab and bevacizumab  
695 for neovascular age-related macular degeneration. *N Engl J Med*. 2011;364(20):1897-

696

1999.

- 697 68. Dugel PU, Koh A, Ogura Y, et al. HAWK and HARRIER: Phase 3, Multicenter,  
698 Randomized, Double-Masked Trials of Brolucizumab for Neovascular Age-Related  
699 Macular Degeneration. *Ophthalmology*. Published online April 12, 2019.  
700 doi:10.1016/j.ophtha.2019.04.017

701

Journal Pre-proof

## **Precis**

We report findings from an artificial intelligence system that automatically quantifies multiple optical coherence tomography features at baseline in patients with neovascular age-related macular degeneration. We make the raw data openly available for further research.

Journal Pre-proof

## Figure legends

**Figure 1.** Fundus photo, optical coherence tomography scan, and corresponding segmentation map for 3 examples. A) MNV in a typical case of neovascular AMD: An 81 year old White female presenting with visual acuity of 63 ETDRS letters. B) Type 3 MNV example: An 83 year old female of other/unknown ethnicity/race presenting visual acuity of 70 ETDRS letters and OCT presenting IRF only. C) Polyp-like example in young patient: A 58 year old Asian female presenting visual acuity of 59 ETDRS letters and OCT showing SRF and suspicious polyp-like lesion. D) Colour key for 13 anatomical features segmented by the segmentation network. AMD = Age related macular degeneration, MNV = Macular neovascularization, ETDRS = Early treatment diabetic retinopathy study, IRF = intraretinal fluid, OCT = optical coherence tomography.

**Figure 2.** Distribution of segmented features volumes stratified by first- and second-treated eyes. The boxes show the median and interquartile range. Whiskers extend to the 5<sup>th</sup> and 95<sup>th</sup> percentiles and beyond this outliers are shown individually. The volume (mm<sup>3</sup>) is distributed across a logarithmic scale; log(zero) is undefined, so zero values were set to the smallest positive value (5.8e-7). NSR = neurosensory retina, RPE = retinal pigment epithelium, IRF = intraretinal fluid, SRF = subretinal fluid, SHRM = subretinal hyperreflective material, HRF = hyperreflective foci, fvPED = fibrovascular pigment epithelium detachment, sPED = serous pigment epithelium detachment.

**Figure 3.** Spearman's correlation between segmented feature volumes and central subfield thickness for A) first and B) second-treated eyes. Tiles display the coefficient  $r_s$ . The upper right half blanks out tiles that have a  $P > 0.05$ ; values are symmetrical otherwise. NSR = neurosensory retina, RPE = retinal pigment epithelium, IRF = intraretinal fluid, SRF = subretinal fluid, SHRM = subretinal hyperreflective material, HRF = hyperreflective foci, fvPED = fibrovascular pigment epithelium detachment, sPED = serous pigment epithelium detachment, CST = central subfield thickness.

**Figure 4.** Distribution of first eye segmented feature volumes stratified by baseline visual acuity (VA) subgroups. VA is stratified into ETDRS letters of 0-35, 36-52, 53-69, and 70 or greater (sTable 4). The boxes show the median and interquartile range. Whiskers extend to the 5<sup>th</sup> and 95<sup>th</sup> percentiles and beyond this outliers are shown individually. The volume is distributed across a logarithmic scale; log(zero) is undefined, so zero values were set to the smallest positive value (5.8e-7). NSR = neurosensory retina, RPE = retinal pigment epithelium, IRF = intraretinal fluid, SRF = subretinal fluid, SHRM = subretinal hyperreflective material, HRF = hyperreflective foci, fvPED = fibrovascular pigment epithelium detachment, sPED = serous pigment epithelium detachment.

**Figure 5.** Distribution of segmented feature volumes in the first eye at baseline stratified by age groups 50-59, 60-69, 70-79, and 80 and above (sTable 4), across a logarithmic scale; log(zero) is undefined, so zero values were set to the smallest positive value (5.8e-7). The boxes show the median and interquartile range. Whiskers extend to the 5<sup>th</sup> and 95<sup>th</sup> percentiles and beyond this outliers are shown individually. NSR = neurosensory retina, RPE = retinal pigment epithelium, IRF = intraretinal fluid, SRF = subretinal fluid, SHRM = subretinal hyperreflective material, HRF = hyperreflective foci, fvPED = fibrovascular pigment epithelium detachment, sPED = serous pigment epithelium detachment.

**Figure 6.** Distribution of segmented feature volumes in the first eyes at baseline stratified by ethnicities: White, Asian, Other or unknown, and Black (sTable 4). The boxes show the median and interquartile range. Whiskers extend to the 5<sup>th</sup> and 95<sup>th</sup> percentiles and beyond this outliers are shown individually. The volume is distributed across a logarithmic scale; log(zero) is undefined, so zero values were set to the smallest positive value (5.8e-7). NSR = neurosensory retina, RPE = retinal pigment epithelium, IRF = intraretinal fluid, SRF = subretinal fluid, SHRM = subretinal hyperreflective material, HRF = hyperreflective foci, fvPED = fibrovascular pigment epithelium detachment, sPED = serous pigment epithelium detachment.

### Demographics of patients included in study

|                                      |                          | First-treated eye | Second-treated eye |
|--------------------------------------|--------------------------|-------------------|--------------------|
| <b>Number of eyes</b>                |                          | 2473              | 493                |
| <b>Gender</b>                        | <b>Female (%)</b>        | 1493 (60.4)       | 342 (69.4)         |
|                                      | <b>Male (%)</b>          | 980 (39.6)        | 151 (30.6)         |
| <b>Race/Ethnicity</b>                | <b>White (%)</b>         | 1319 (53.3)       | 290 (58.8)         |
|                                      | <b>Asian (%)</b>         | 257 (10.4)        | 40 (8.1)           |
|                                      | <b>Black (%)</b>         | 57 (2.3)          | 5 (1.0)            |
|                                      | <b>Other/Unknown (%)</b> | 840 (34.0)        | 158 (32.0)         |
| <b>Age (years)</b>                   | <b>Mean (SD)</b>         | 79.3 (8.6)        | 81.4 (7.9)         |
|                                      | <b>50-59 (%)</b>         | 60 (2.4)          | 3 (0.6)            |
|                                      | <b>60-69 (%)</b>         | 289 (11.7)        | 40 (8.1)           |
|                                      | <b>70-79 (%)</b>         | 791 (32.0)        | 139 (28.2)         |
|                                      | <b>≥80 (%)</b>           | 1332 (53.9)       | 311 (63.1)         |
| <b>Visual Acuity (ETDRS letters)</b> | <b>Mean (SD)</b>         | 54.0 (16.1)       | 62.5 (13.2)        |
|                                      | <b>0-35 (%)</b>          | 385 (15.6)        | 27 (5.5)           |
|                                      | <b>36-52 (%)</b>         | 506 (20.5)        | 64 (13.0)          |
|                                      | <b>53-69 (%)</b>         | 885 (35.8)        | 202 (41.0)         |
|                                      | <b>≥70 (%)</b>           | 471 (19.0)        | 194 (39.4)         |
|                                      | <b>Unknown VA (%)</b>    | 226 (9.2)         | 6 (1.2)            |

**Table 1.** Demographics of the dataset. SD = standard deviation, ETDRS = Early treatment diabetic retinopathy study, VA = visual acuity.

### Baseline mean and median volumes of OCT segmented features in first- and second-treated eyes

| Segmented feature                | Mean (standard deviation) at first injection |                      | Median (interquartile range) at first injection |                            | Mann-Whitney U test P-value |
|----------------------------------|--|----------------------|---|----------------------------|-----------------------------|
|                                  | First-treated eye                            | Second-treated eye   | First-treated eye                               | Second-treated eye         |                             |
| NSR volume (mm <sup>3</sup> )    | <b>9.485 (1.013)</b>                         | 9.269 (0.775)        | <b>9.445 (8.905–9.983)</b>                      | 9.306 (8.790–9.767)        | <0.001                      |
| RPE volume (mm <sup>3</sup> )    | <b>0.806 (0.094)</b>                         | 0.794 (0.088)        | <b>0.808 (0.763–0.857)</b>                      | 0.800 (0.755–0.845)        | 0.002                       |
| IRF volume (mm <sup>3</sup> )    | <b>0.118 (0.309)</b>                         | 0.073 (0.196)        | <b>0.007 (0.000–0.090)</b>                      | 0.003 (0.000–0.049)        | <0.001                      |
| SRF volume (mm <sup>3</sup> )    | <b>0.455 (0.733)</b>                         | 0.258 (0.532)        | <b>0.183 (0.022–0.562)</b>                      | 0.054 (0.006–0.252)        | <0.001                      |
| SHRM volume (mm <sup>3</sup> )   | <b>0.380 (0.661)</b>                         | 0.148 (0.283)        | <b>0.135 (0.024–0.445)</b>                      | 0.054 (0.007–0.186)        | <0.001                      |
| HRF volume (mm <sup>3</sup> )    | <b>0.003 (0.008)</b>                         | 0.002 (0.006)        | <b>0.001 (0.000–0.002)</b>                      | 0.001 (0.000–0.002)        | 0.318                       |
| Drusen volume (mm <sup>3</sup> ) | 0.036 (0.085)                                | <b>0.060 (0.080)</b> | 0.010 (0.002–0.036)                             | <b>0.031 (0.009–0.080)</b> | <0.001                      |
| fvPED volume (mm <sup>3</sup> )  | <b>0.765 (1.305)</b>                         | 0.491 (0.935)        | <b>0.283 (0.089–0.815)</b>                      | 0.200 (0.062–0.523)        | <0.001                      |
| sPED volume (mm <sup>3</sup> )   | <b>0.004 (0.023)</b>                         | 0.002 (0.012)        | <b>0.000 (0.000–0.001)</b>                      | 0.000 (0.000–0.000)        | <0.001                      |
| CST (μm)                         | <b>347.1 (114.3)</b>                         | 306.1 (85.1)         | <b>325.8 (266.6–405.0)</b>                      | 295.0 (253.9–340.3)        | <0.001                      |

**Table 2.** Mean and median volumes with standard deviations and interquartile range of segmented features in first- and second-treated eyes at first injection. Segmented voxels were converted into mm<sup>3</sup>. P-values were considered significant at ≤0.05. NSR = neurosensory retina, RPE = retinal pigment epithelium, IRF = intraretinal fluid, SRF = subretinal fluid, PED = pigment epithelium detachment, SHRM = subretinal hyperreflective material, HRF = hyperreflective foci, fvPED = fibrovascular PED, sPED = serous PED, CST = central subfield thickness.

**Univariable linear regression and Spearman's rank correlation coefficient assessing the relationship between volumes and visual acuity, and age and volumes, in first-treated eyes.**

| Volumes (X),<br>Visual acuity (Y) | Linear regression (ordinary least squares) |             |           |                   | Spearman's rank |                   |
|-----------------------------------|--|-------------|-----------|-------------------|-----------------|-------------------|
|                                   | R-squared                                  | Coefficient | Intercept | P-value           | $r_s$           | P-value           |
| CST**                             | 0.107                                      | -0.045      | 69.855    | <b>&lt;0.001*</b> | -0.306          | <b>&lt;0.001*</b> |
| SHRM                              | 0.082                                      | -7.013      | 56.616    | <b>&lt;0.001*</b> | -0.380          | <b>&lt;0.001*</b> |
| IRF                               | 0.054                                      | -11.939     | 55.410    | <b>&lt;0.001*</b> | -0.347          | <b>&lt;0.001*</b> |
| RPE                               | 0.027                                      | 30.273      | 29.548    | <b>&lt;0.001*</b> | 0.169           | <b>&lt;0.001*</b> |
| fvPED                             | 0.022                                      | -1.824      | 55.389    | <b>&lt;0.001*</b> | -0.210          | <b>&lt;0.001*</b> |
| NSR                               | 0.015                                      | -1.957      | 72.530    | <b>&lt;0.001*</b> | -0.088          | <b>&lt;0.001*</b> |
| SRF                               | 0.008                                      | -1.947      | 54.866    | <b>&lt;0.001*</b> | -0.090          | <b>&lt;0.001*</b> |
| Drusen                            | 0.008                                      | 16.637      | 53.370    | <b>&lt;0.001*</b> | 0.144           | <b>&lt;0.001*</b> |
| HRF                               | 0.005                                      | -141.423    | 54.456    | <b>&lt;0.001*</b> | -0.092          | <b>&lt;0.001*</b> |
| sPED                              | 0.005                                      | 50.395      | 53.753    | <b>&lt;0.001*</b> | 0.134           | <b>&lt;0.001*</b> |
| Age (X), Volumes<br>(Y)           | Linear regression (ordinary least squares) |             |           |                   | Spearman's rank |                   |
|                                   | R-squared                                  | Coefficient | Intercept | P-value           | $r_s$           | P-value           |
| RPE                               | 0.061                                      | -0.003      | 1.005     | <b>&lt;0.001*</b> | -0.257          | <b>&lt;0.001*</b> |
| sPED                              | 0.013                                      | 0.000       | 0.028     | <b>&lt;0.001*</b> | -0.218          | <b>&lt;0.001*</b> |
| NSR                               | 0.010                                      | -0.012      | 10.415    | <b>&lt;0.001*</b> | -0.114          | <b>&lt;0.001*</b> |
| SRF                               | 0.006                                      | -0.007      | 0.988     | <b>&lt;0.001*</b> | -0.140          | <b>&lt;0.001*</b> |
| IRF                               | 0.004                                      | 0.002       | -0.069    | <b>0.001*</b>     | 0.171           | <b>&lt;0.001*</b> |
| HRF                               | 0.001                                      | 0.000       | 0.001     | 0.064             | 0.056           | <b>0.005</b>      |
| fvPED                             | 0.001                                      | -0.004      | 1.091     | 0.178             | 0.020           | 0.323             |
| SHRM                              | 0.001                                      | 0.002       | 0.223     | 0.200             | 0.026           | 0.203             |
| CST**                             | 0.000                                      | -0.234      | 372.987   | 0.391             | -0.011          | 0.578             |
| Drusen                            | 0.000                                      | 0.000       | 0.028     | 0.603             | 0.117           | <b>&lt;0.001*</b> |

**Table 3.** Univariable linear regression and Spearman's rank correlation coefficient assessing the relationship between volumes and visual acuity, and age and volumes, in first-treated eyes. P-values are given before Bonferroni correction. Bolded values were significant at  $P \leq 0.05$ . Asterisk (\*) P-values remain significant at  $P \leq 0.005$  after Bonferroni correction. \*\*CST measures thickness and not volume. CST = Central subfield thickness,

NSR = neurosensory retina, HRF = Hyperreflective foci, RPE = retinal pigment epithelium, sPED = serous pigment epithelium detachment, fvPED = fibrovascular pigment epithelium detachment.

Journal Pre-proof

**Univariable linear regression and Spearman's rank correlation coefficient assessing the relationship between volumes and visual acuity, and age and volumes, in second-treated eyes.**

| Volumes (X),<br>Visual acuity (y) | Linear regression (ordinary least squares) |             |           |                   | Spearman's rank |                   |
|-----------------------------------|--|-------------|-----------|-------------------|-----------------|-------------------|
|                                   | R-squared                                  | Coefficient | Intercept | P-value           | $r_s$           | P-value           |
| SHRM                              | 0.122                                      | -16.23      | 64.976    | <b>&lt;0.001*</b> | -0.293          | <b>&lt;0.001*</b> |
| RPE                               | 0.067                                      | 39.859      | 30.888    | <b>&lt;0.001*</b> | 0.239           | <b>&lt;0.001*</b> |
| CST**                             | 0.024                                      | -0.02       | 69.932    | <b>&lt;0.001*</b> | -0.152          | <b>0.001*</b>     |
| IRF                               | 0.023                                      | -10.17      | 63.315    | <b>&lt;0.001*</b> | -0.224          | <b>&lt;0.001*</b> |
| fvPED                             | 0.020                                      | -2.00       | 63.549    | <b>0.002*</b>     | -0.142          | <b>0.002*</b>     |
| NSR                               | 0.016                                      | 2.20        | 42.140    | <b>0.006</b>      | 0.114           | <b>0.012</b>      |
| SRF                               | 0.014                                      | -2.89       | 63.318    | <b>0.010</b>      | -0.020          | 0.659             |
| Drusen                            | 0.010                                      | 16.72       | 61.573    | <b>0.028</b>      | 0.118           | <b>0.009</b>      |
| HRF                               | 0.004                                      | -139.85     | 62.853    | 0.170             | -0.089          | -0.089            |
| sPED                              | 0.002                                      | 47.21       | 62.466    | 0.354             | 0.136           | <b>0.003*</b>     |
|                                   |  |             |           |                   |                 |                   |
| Age (X), Volumes<br>(y)           | Linear regression (ordinary least squares) |             |           |                   | Spearman's rank |                   |
|                                   | R-squared                                  | Coefficient | Intercept | P-value           | $r_s$           | P-value           |
| RPE                               | 0.031                                      | -0.002      | 0.952     | <b>&lt;0.001*</b> | -0.245          | <b>&lt;0.001*</b> |
| NSR                               | 0.031                                      | -0.017      | 10.670    | <b>&lt;0.001*</b> | -0.171          | <b>&lt;0.001*</b> |
| IRF                               | 0.014                                      | 0.003       | -0.167    | <b>0.008</b>      | 0.190           | <b>&lt;0.001*</b> |
| sPED                              | 0.013                                      | 0.000       | 0.016     | <b>0.011</b>      | -0.209          | <b>&lt;0.001*</b> |
| SRF                               | 0.012                                      | -0.007      | 0.849     | <b>0.016</b>      | -0.174          | <b>&lt;0.001*</b> |
| fvPED                             | 0.009                                      | -0.011      | 1.398     | <b>0.036</b>      | -0.111          | <b>0.014</b>      |
| CST**                             | 0.002                                      | -0.445      | 348.885   | 0.367             | -0.031          | 0.493             |
| HRF                               | 0.001                                      | 0.000       | 0.004     | 0.483             | 0.103           | <b>0.022</b>      |
| SHRM                              | 0.000                                      | 0.000       | 0.187     | 0.767             | -0.034          | 0.453             |
| Drusen                            | 0.000                                      | 0.000       | 0.059     | 0.978             | 0.068           | 0.132             |

**Table 4.** Univariable linear regression and Spearman's rank correlation coefficient assessing the relationship between volumes and visual acuity, and age and volumes, in second-treated eyes. P-values are given before Bonferroni correction. \*Remains significant at  $P \leq 0.005$  after Bonferroni correction. \*\*CST measures thickness and not volume. CST =

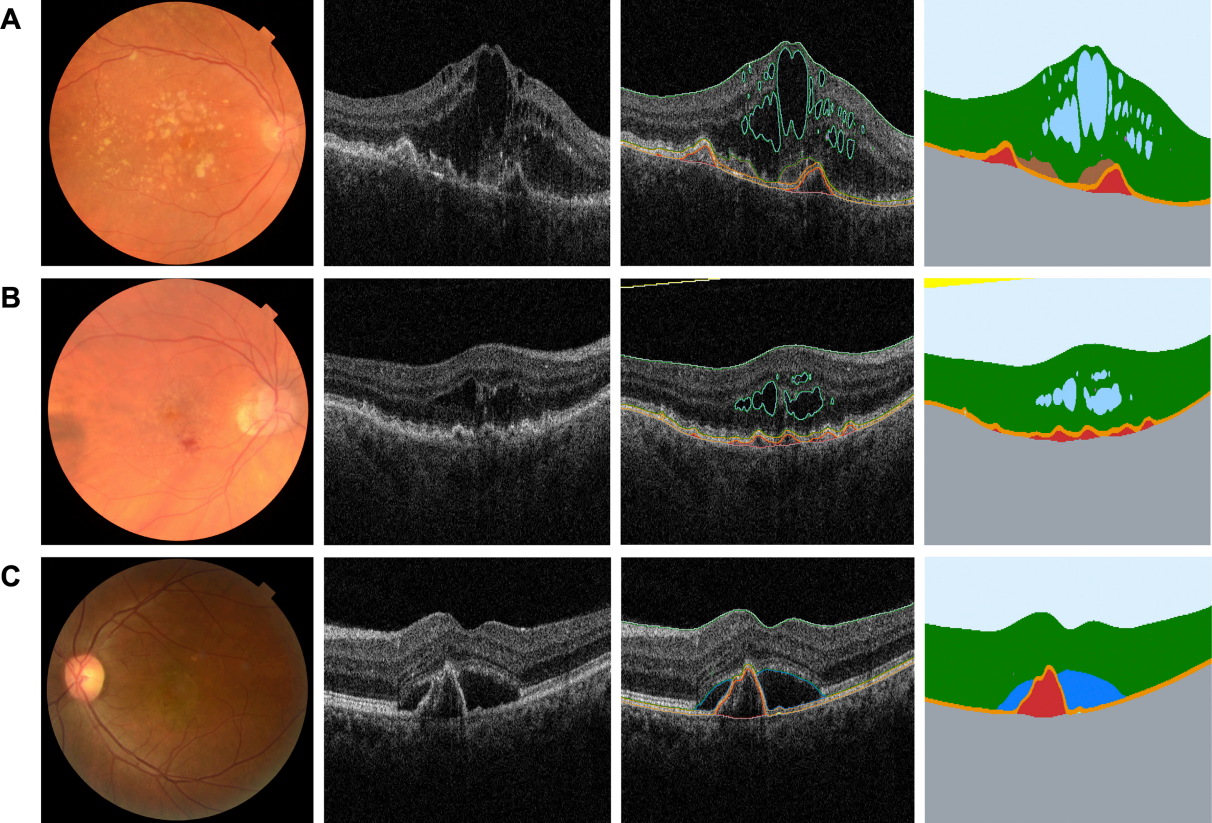
hyperreflective material, NSR = neurosensory retina, HRF = Hyperreflective foci, RPE = retinal pigment epithelium, sPED = serous pigment epithelium detachment, fvPED = fibrovascular pigment epithelium detachment.

Journal Pre-proof

**Relative presence of IRF and SRF at baseline**

| Parameter                     | First-treated eye<br>(total n = 2473 eyes) | Second-treated eye<br>(total n = 493 eyes) |
|-------------------------------|--|--|
| IRF [n, (%)]                  | 1653 (66.8)                                | 297 (60.2)                                 |
| SRF [n, (%)]                  | 2045 (82.7)                                | 358 (72.6)                                 |
| IRF only without SRF [n, (%)] | 301 (12.2)                                 | 105 (21.3)                                 |
| SRF only without IRF [n, (%)] | 693 (28.0)                                 | 166 (33.7)                                 |
| IRF and SRF [n, (%)]          | 1352 (54.7)                                | 192 (38.9)                                 |
| Neither IRF nor SRF [n, (%)]  | 127 (5.1)                                  | 30 (6.1)                                   |

**Table 5.** Relative presence/volumes of IRF and SRF at baseline. IRF and SRF are defined as present at  $\geq 453$  voxels ( $0.0007\text{mm}^3$ ) and  $\geq 5199$  ( $0.0075\text{mm}^3$ ) voxels, respectively. IRF = intraretinal fluid, SRF = subretinal fluid.

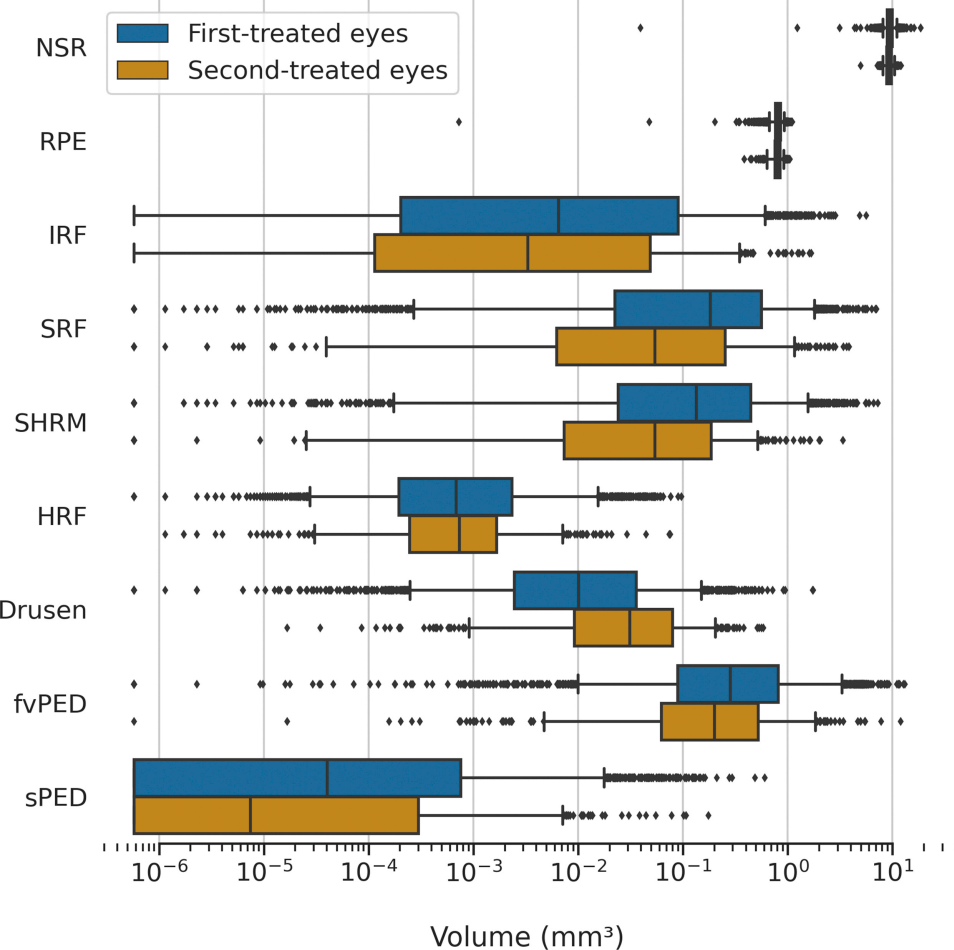


**D**

- Light blue: Vitreous and subhyaloid
- Cyan: Posterior hyaloid
- Dark blue: Epiretinal membrane
- Green: Neurosensory retina
- Light green: Intraretinal fluid

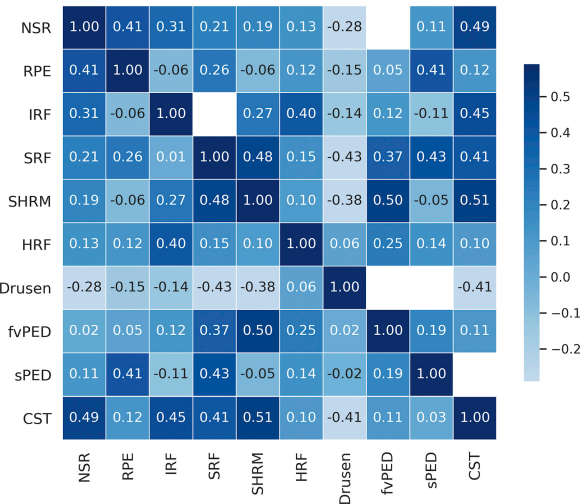
- Blue: Subretinal fluid
- Brown: Subretinal hyperreflective material
- Purple: Hyperreflective foci
- Orange: Retinal pigment epithelium

- Yellow: Drusen
- Light green: Serous PED
- Red: Fibrovascular PED
- Grey: Choroid and outer layers



**A**

First-treated eyes: Correlations between segmented features

**B**

Second-treated eyes: Correlations between segmented features

